www.acsnano.org

# van der Waals SWCNT@BN Heterostructures Synthesized from Solution-Processed Chirality-Pure Single-Wall Carbon Nanotubes

Chiyu Zhang, Jacob Fortner, Peng Wang, Jeffrey A. Fagan, Shuhui Wang, Ming Liu, Shigeo Maruyama, and YuHuang Wang\*



Downloaded via UNIV OF MARYLAND COLG PARK on November 29, 2022 at 19:32:34 (UTC). See https://pubs.acs.org/sharingguidelines for options on how to legitimately share published articles.

Cite This: ACS Nano 2022, 16, 18630-18636



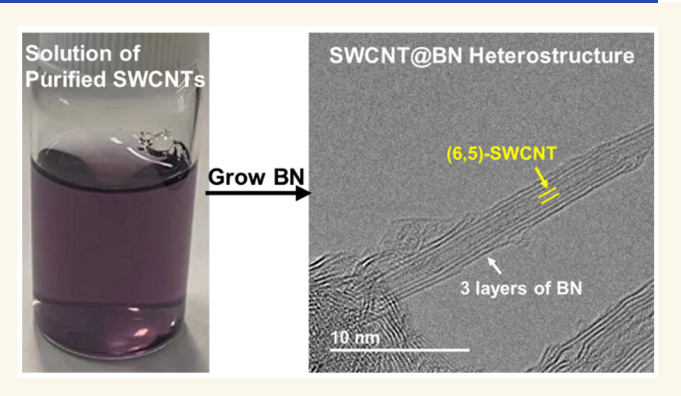
**ACCESS** 

III Metrics & More

Article Recommendations

Supporting Information

ABSTRACT: Single-wall carbon nanotubes in boron nitride (SWCNT@BN) are one-dimensional van der Waals heterostructures that exhibit intriguing physical and chemical properties. As with their carbon nanotube counterparts, these heterostructures can form from different combinations of chiralities, providing rich structures but also posing a significant synthetic challenge to controlling their structure. Enabled by advances in nanotube chirality sorting, clean removal of the surfactant used for solution processing, and a simple method to fabricate free-standing submonolayer films of chirality pure SWCNTs as templates for the BN growth, we show it is possible to directly grow BN on chirality enriched SWCNTs from solution processing to form van der Waals heterostructures. We



further report factors affecting the heterostructure formation, including an accelerated growth rate in the presence of  $H_2$ , and significantly improved crystallization of the grown BN, with the BN thickness controlled down to one single BN layer, through the presence of a Cu foil in the reactor. Transmission electron microscopy and electron energy-loss spectroscopic mapping confirm the synthesis of SWCNT@BN from the solution purified nanotubes. The photoluminescence peaks of both (7,5)- and (8,4)-SWCNT@BN heterostructures are found to redshift (by  $\sim$ 10 nm) relative to the bare SWCNTs. Raman scattering suggests that the grown BN shells pose a confinement effect on the SWCNT core.

KEYWORDS: single-wall carbon nanotube, boron nitride, van der Waals heterostructure, chemical vapor deposition, solution processing, photoluminescence

🔰 ingle-wall carbon nanotube in boron nitride nanotube (SWCNT@BN) heterostructures have recently emerged as a materials platform to study the physics of manipulated crystals, heterojunction diodes, and enhanced thermal conductors.3 The SWCNTs feature ballistic transport properties, 4,5 while the BN is chemically inert and has a large bandgap (5.96 eV).<sup>6,7</sup> This combination delivers enhanced transport as well as thermal and chemical stability. However, these heterostructures inherit the (n,m) chirality challenge of SWCNTs, as they are synthesized through a two-step chemical vapor deposition (CVD) process, in which the carbon nanotubes are first synthesized and followed by the growth of BN as a shell coating. As chirality control is currently a challenge for SWCNT synthesis, the resulting SWCNT@BN van der Waals heterostructures are a complex mixture, which prevents applications and studies requiring defined structures and properties.9-11

While SWCNTs are generally synthesized in a mixture of chiralities, solution processing has enabled the purification and sorting of SWCNTs with single chirality purity. <sup>12–14</sup> In these approaches, SWCNTs are dispersed in solution with the aid of surfactants and polymers, aiding individualization but also introducing additional components undesirable for heterostructure growth. It is typically difficult to remove these surfactants and polymers from the dispersed SWCNTs, and any residues make the clean SWCNT surface inaccessible, which is required for the growth of perfect outer crystals. BN

Received: July 18, 2022
Accepted: November 4, 2022
Published: November 8, 2022





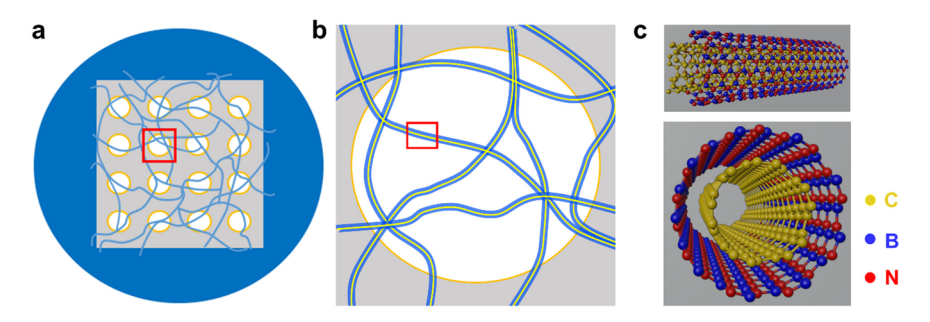


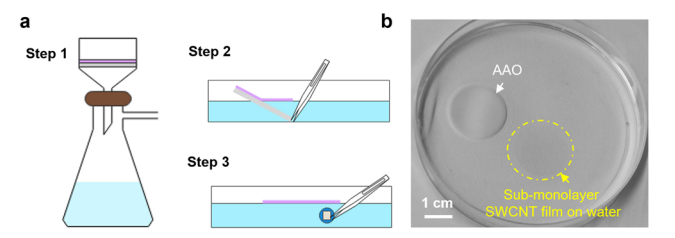
Figure 1. Overview of the SWCNT@BN semiconductor networks. Schematic of (a) SWCNT@BN suspended on a holey  $Si_3N_4$  grid and (b) across a hole (enlarged drawing of the red rectangle region in (a)), where the BN shell is shown in blue and SWCNTs is yellow. (c) Atomic model of a SWCNT wrapped with a BN shell.

usually grows one or two layers from a single starting point on a clean SWCNT surface, while on a contaminated surface, BN forms polycrystalline shells as contaminations may serve as multiple nucleation sites. <sup>15,16</sup> Recently, several of the authors developed a thermally removable surfactant ammonium deoxycholate (ADC)<sup>17</sup> that can be removed cleanly to allow the synthesis of chirality pure SWCNT@BN heterostructures. In this study, we incorporate this advance and demonstrate the successful growth of BN on solution-processed nanotubes of purified chirality.

We use established methods such as aqueous two-phase extraction (ATPE)<sup>18</sup> to sort polydisperse SWCNTs populations for desired chirality species, including (6,5), (7,5), and (8,4) used in this study. The surfactants and polymers from this process were then thoroughly exchanged for ADC using ultrafiltration and volumetric exchange with ADC solution; clean submonolayer films were generated by filtration. We then transferred and suspended ultrathin and free-standing films of the purified SWCNT solutions on a Si<sub>3</sub>N<sub>4</sub> TEM grid (Figure 1). BN was grown on the suspended SWCNT templates through a CVD process. We found the growth rate was accelerated by  $\sim$ 6 times when pure H<sub>2</sub> was used as the carrier gas in place of the 3 vol/vol % H<sub>2</sub>/Ar source and the BN crystallization can be improved using a Cu catalyst. The BN coating was characterized by transmission electron microscopy (TEM) and electron energy-loss spectroscopic (EELS) mapping. Hyperspectral imaging confirms the synthesis of photoluminescent (7,5)-SWCNT@BNs.

#### **RESULTS AND DISCUSSION**

We developed a simple method to fabricate free-standing submonolayer films from solution-processed SWCNTs and deposit the film on a Si<sub>3</sub>N<sub>4</sub> TEM grid to suspend the SWCNTs, which serve as templates for BN growth (Figure 2). The film was made on an anodic aluminum oxide (AAO) membrane through vacuum filtration. We removed the majority of surfactant with copious water and isopropanol, rinsed the film with HCl solution, released the SWCNT thin film from the AAO by immersing the membrane in water, and finally transferred the SWCNT film onto a Si<sub>3</sub>N<sub>4</sub> grid by inserting the grid into water below the floating film and picking it up (Figure 2a). Figure 2b shows the freed thin SWCNT film floating on the water surface. Figure 2c shows a TEM image of the homogeneous SWCNT network suspended across a 20  $\mu$ m diameter pore. Compared with traditional filtration methods which involve dissolving the filtration membrane to release the SWCNT film, <sup>19</sup> our method is cleaner and simpler.



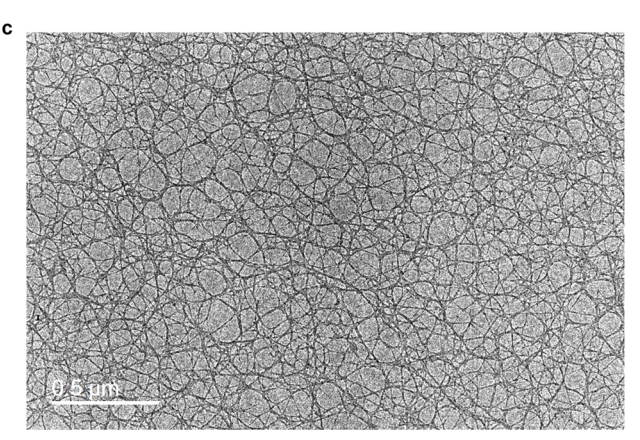


Figure 2. Free-standing, submonolayer thin film of SWCNTs from solution processing. (a) Schematic of key steps. Step 1: Vacuum filtration to form a SWCNT film (purple) on an AAO membrane (gray). Step 2: Immerse the AAO membrane into water to release the SWCNT film, which floats on the water surface. Step 3: Insert a  $\mathrm{Si}_3\mathrm{N}_4$  grid below the floating SWCNT film to pick up the SWCNT film. (b) Photograph of a SWCNT thin film floating on the water surface. Note the separated AAO membrane. (c) TEM image of the SWCNT film suspended across the pore of a  $\mathrm{Si}_3\mathrm{N}_4$  grid.

Importantly, we note that the HCl treatment is critical to achieving the release of the submonolayer SWCNT film from the AAO membrane. Without the acid treatment, the film cannot be released when immersed in water. Although the detailed mechanism underlying this phenomenon requires further studies, we can reason that this submonolayer release occurs due to HCl chemistry at the AAO-SWCNT interface. Because the AAO membrane is hydrophilic and nanoporous, a hydration layer can form on the surface. On the other hand, the SWCNT thin film exhibits hydrophobicity as the surfactant is removed from the SWCNTs. The hydration layer prevents the AAO surface from direct contact with the SWCNT film. When we added HCl, the AAO membrane was etched by HCl, as evidenced by its complete dissolution if left in the acid for 12 h, allowing water to enter the interlayer during immersion.

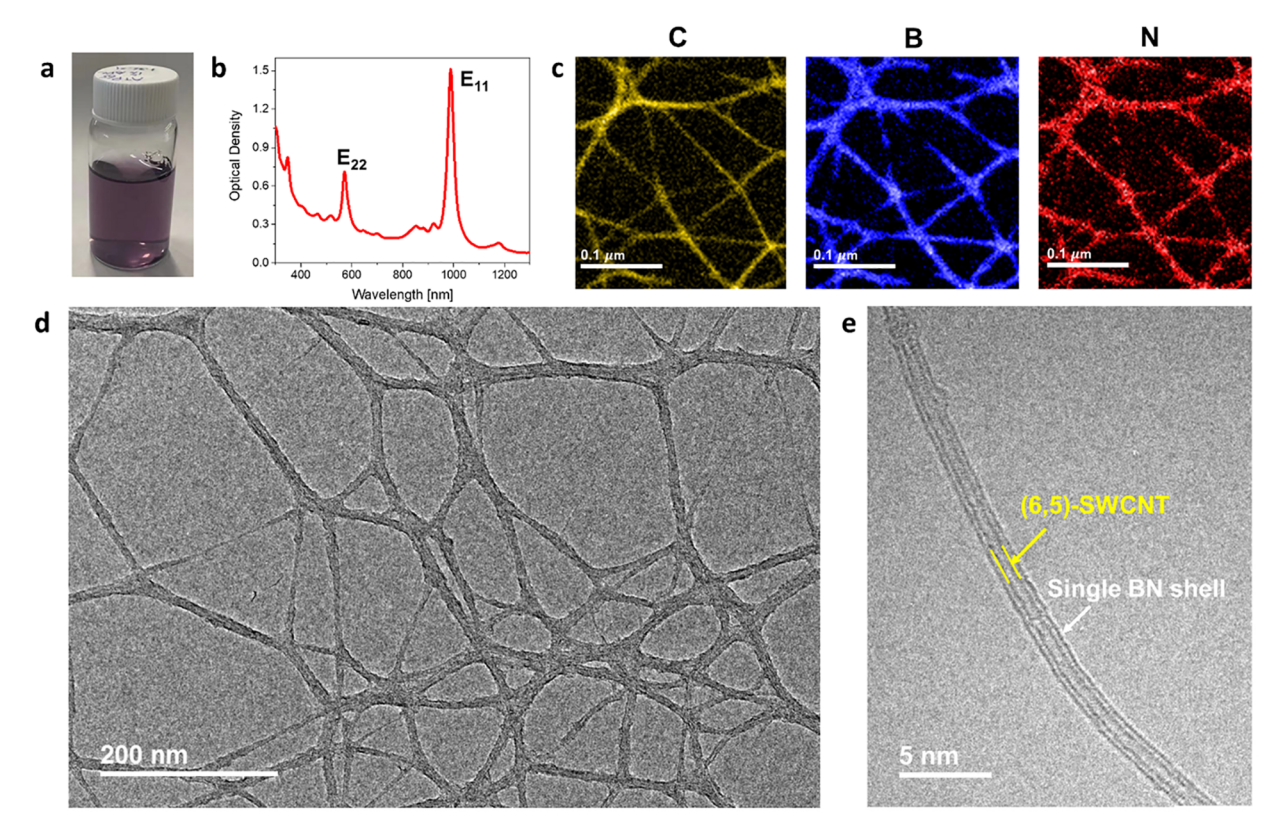


Figure 3. Growth of BN on SWCNT templates. (a) Photograph and (b) absorption spectrum of purified (6,5)-SWCNTs in 10 g/L ADC aqueous solution ( $E_{11}$  at 985 nm optical density = 1.52). (c) EELS mappings of carbon, boron, and nitrogen of (6,5)-SWCNT@BN networks. TEM images of (d) SWCNT@BN networks and (e) an individual SWCNT (diameter = 0.71 nm) enclosed by a single BN shell. The (6,5)-SWCNT film has optical transmittance of 93.1% at 985 nm ( $E_{11}$ ).

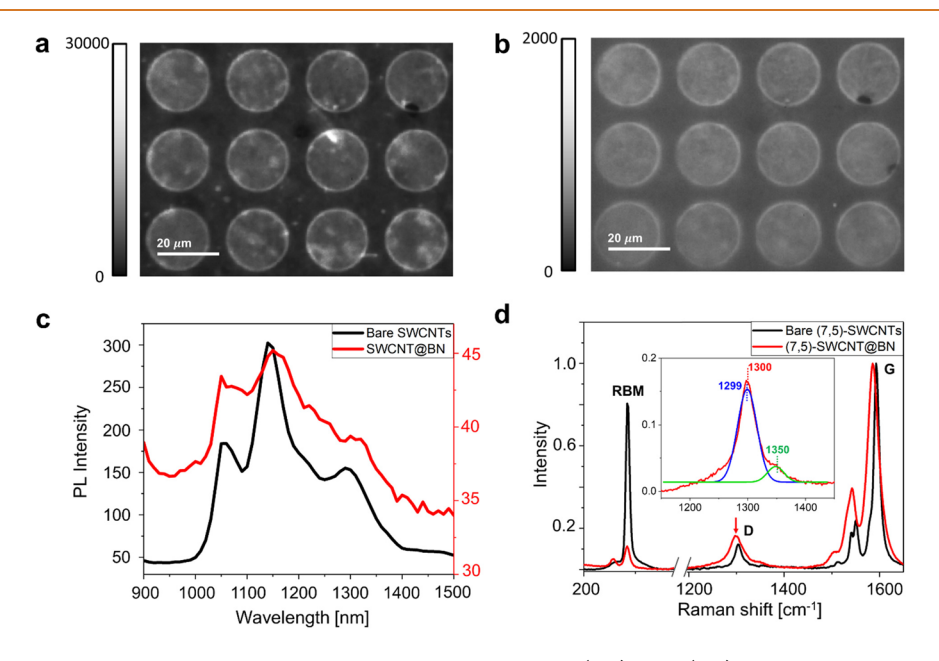


Figure 4. Optical characterization of SWCNT@BN. Hyperspectral PL images of (7,5)- and (8,4)-enriched SWCNT film (a) before and (b) after BN growth. (c) PL spectra and (d) resonant Raman scattering of (7,5)-SWCNTs before (black) and after (red) BN growth. The 1300 cm<sup>-1</sup> band is spectrally fitted by the D peak of SWCNTs (blue curve in inset, at 1299 cm<sup>-1</sup>) and B-N stretching peak (green, at 1350 cm<sup>-1</sup>). The Raman excitation line is 632.8 nm, which resonantly excites (7,5)-SWCNT. The SWCNT film (transmittance = 86.3% at the  $E_{11}$  absorption peak of (7,5)) was prepared from a 200  $\mu$ L,OD 1.81 solution. The PL images were collected using a 50× objective, along with a continuous wave laser at 730 nm at a power density of  $\approx$ 75 W/cm<sup>2</sup> as the excitation light source.

Therefore, the SWCNT film detaches from the AAO surface easily and floats on the water.

To grow BN on purified SWCNT films, we obtained a solution of semiconducting SWCNTs with single chirality

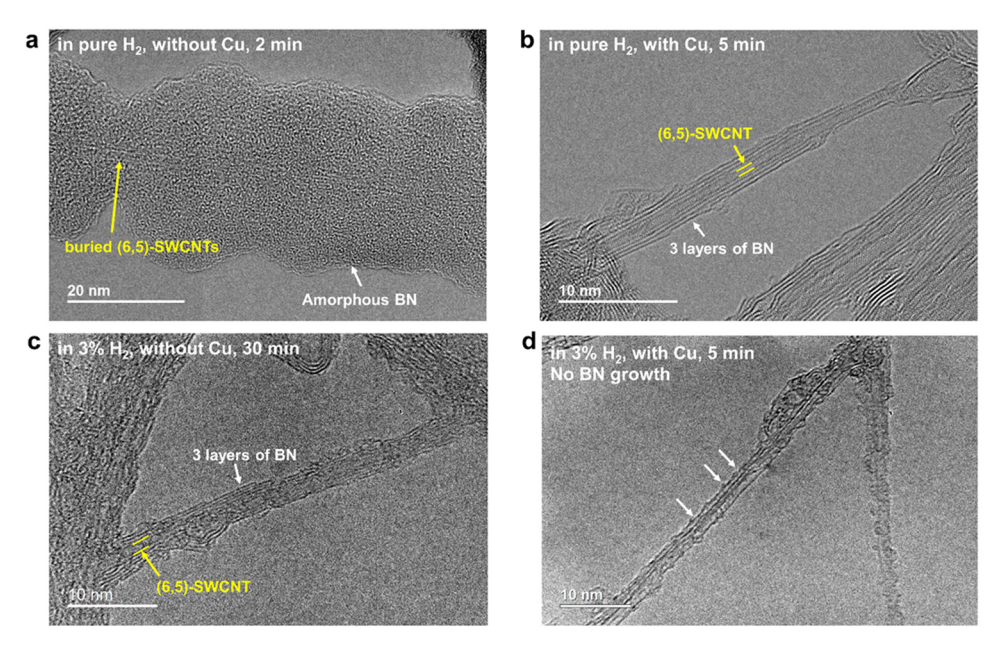


Figure 5. TEM images of (6,5)-SWCNTs (a) coated by thick and amorphous BN after 2 min growth without Cu and and (b) enclosed by 1–3 layers of crystalline BN after 5 min growth with Cu at 1065 °C in pure  $H_2$ . (c) (6,5)-SWCNTs enclosed by 1–3 layers of BN after 30 min growth without Cu and (d) no BN layer forms after 5 min growth with Cu at 1065 °C in 3 vol/vol %  $H_2$ . Yellow arrows show the (6,5)-SWCNTs, and white arrows indicate the amorphous, crystallized, or undeveloped BN.

(6,5) (diameter = 0.78 nm) by ATPE (Figure 3a). During ATPE, individual SWCNTs selectively partition between the two polymer-aqueous phases of different hydrophobicity in a manner that is tunable with respect to SWCNT chirality by controlling the concentration of competing cosurfactants. Through stepwise tuning of the concentration of surfactants, pure semiconducting SWCNTs with tailored chirality were sorted out. Figure 3b shows the absorption spectrum of the sorted (6,5)-SWCNTs. In order to avoid surfactant residues hindering the BN coating, we exchanged the surfactants of the ATPE-sorted (6,5)-SWCNT solution to a thermally removable surfactant, ADC<sup>17</sup> by ultrafiltration. A free-standing submonolayer film (transmittance 93.1% at the E<sub>11</sub> wavelength) was fabricated from the chirality pure (6,5)-SWCNTs and transferred on a Si<sub>3</sub>N<sub>4</sub> grid. We placed the grid (Figure S1c) on a quartz chip and tented with a Cu foil (Figure S1b), which was placed in a tube furnace for CVD deposition (Figure S1a). We used ammonia borane as a precursor to provide boron and nitrogen, with the source located upstream of the grid outside of the primary furnace hot zone. When the temperature of the grid increased to 1065 °C, the ammonia borane was heated to 65 °C. Sublimated ammonia borane was carried by H<sub>2</sub> to deposit on the SWCNT templates to form the SWCNT@BN heterostructure. We confirmed the coating was BN by EELS mapping (Figure 3c). In Figure 3d,e, we used TEM to characterize the morphology of the resulting SWCNT@BN networks, revealing individual SWCNTs coated with a uniform BN shell. Based on the statistics from 56 individual (6,5)-SWCNT@BN heterostructures, we found that single SWCNTs are coated by 1-3 layers of BN, while small bundles consisting of two SWCNTs are coated by 2-6 layers of BN (Figure S2). It is noted that the BN shell protects SWCNTs from external attacks such as electron beams. Naked (6,5)-SWCNT can be damaged by the electron beam during TEM characterization, while those covered by a BN shell were protected (Figure S3).

We also fabricated SWCNT@BN heterostructures using (7,5) and (8,4)-enriched SWCNTs (diameter = 0.83 nm). Figure S4 shows absorption spectrum of the (7,5) and (8,4)enriched SWCNTs. Before annealing, the ADC surfactant was observed on the SWCNTs (Figure S5a). After annealing in 3 vol/vol % H<sub>2</sub>/Ar for 30 min at 1065 °C, which is the same condition used for BN growth, the surfactant was removed (Figure S5b). Successful growth of BN coating is confirmed by TEM and EELS (in Figure S6). Optical properties of the semiconducting SWCNTs before and after being wrapped by the BN layers were characterized by hyperspectral photoluminescence (PL) imaging and resonant Raman scattering. Figure 4a shows broadband PL images of the bare (7,5)- and (8,4)-enriched SWCNT film suspended on the 20  $\mu$ m pores of the Si<sub>3</sub>N<sub>4</sub> grid. After the BN growth, the SWCNT film PL intensity decreased by an order of magnitude (Figure 4b). The PL spectrum (Figure 4c) demonstrates that (7,5) and (8,4)-SWCNT@BN heterostructures possess a similar E<sub>11</sub> peak to their bare SWCNTs, respectively, but with an ≈10 nm red shift. However, PL of the (6,5)-SWCNTs disappeared after the BN coating (Figure S7). Because smaller diameter SWCNTs are more chemically vulnerable and prone to damage, we hypothesize that the PL of the (6,5)-SWCNTs accumulated structural damage from the high temperature environment during BN growth. This idea was corroborated by annealing a (6,5)-SWCNT film to the same temperature for BN growth (1065 °C) without the presence of the ammonia borane precursor. The PL signal, as shown in Figure S8, was completely suppressed after the treatment, while scanning electron microscopy confirmed the continued existence of (6,5)-SWCNTs. In Figure 4d, resonant Raman scattering resolves the typical radial breathing mode of (7,5)-SWCNTs at 285 cm<sup>-1</sup> after BN coating, while its intensity decreases significantly. This spectral change may arise from the radial confinement and strain posed by the grown BN shells.<sup>21</sup> The tangential vibrational modes (G peak) of SWCNTs downshift by  $\approx 7 \text{ cm}^{-1}$  (from 1593 to 1586 cm<sup>-1</sup>) after BN coating. The

downshift can be attributed to uniaxial distortion of SWCNTs caused by the difference in thermal expansion of the SWCNT and BN.¹ Furthermore, the D peak of SWCNTs becomes wider and stronger, signaling contributions from the B–N stretching at 1350 cm⁻¹ that overlaps with the D peak at 1299 cm⁻¹.²22-24 After the BN growth, a peak also emerges at 800 cm⁻¹ (Figure S9), which corresponds to the B–N bending mode.³,25

We observed accelerated growth of BN by using pure H<sub>2</sub> as carrier gas in place of 3 vol./vol % H<sub>2</sub>/Ar used by some of us in previous experiments<sup>1,2,26</sup> and improved BN crystallization with Cu catalyst, overcoming the slow growth rate of BN. 15 In pure H<sub>2</sub>, thick and amorphous BN wrapped (6,5)-SWCNTs in 2 min at 1065 °C (Figure 5a), while 1-3 layers of BN grow on (6,5)-SWCNTs in 3 vol/vol %  $H_2$ /Ar for 30 min (Figure 5c). We also found that the BN crystallization grown in pure H<sub>2</sub> can be improved by using Cu foil. As shown in Figure 5b, we observed 1-3 crystalline layers of BN instead of amorphous ones when Cu was used. With Cu, the SWCNT@BN exhibits more uniform morphology by TEM (Figure S10) and EELS spectra of boron atoms present an increased intensity ratio of the  $\pi^*$  peak to the  $\sigma^*$  peak. Cu has been widely used to catalyze the growth of hexagonal boron nitride and boron nitride nanotubes since it is able to dissolve both boron and nitrogen with equivalent proportions. <sup>27,28</sup> At 1065 °C, which is close to the melting point of Cu (1083 °C), we hypothesize that Cu deposited on the grid or in the gas phase catalyzes decomposition of the ammonia borane and BN growth, resulting in the more homogeneous morphology we observed. Interestingly, Cu does not accelerate, but rather it seems to slow down the growth rate of BN. When growing in 3 vol/vol % H<sub>2</sub>/Ar, with Cu in 5 min, BN did not form a shell to wrap the SWCNTs completely (Figure 5d) and the EELS signal of B, N was very weak (Figure S11). We further note that the growth rate of BN is impacted by the curvature of the SWCNT templates. When BN grew with the Cu catalyst in pure H<sub>2</sub> at 1070 °C for 2 min, an individual EC 2.0 SWCNT (diameter =  $\approx$ 2 nm) was wrapped by 1–2 BN layers, while  $\sim$ 4 BN layers grew on a bundle of EC2.0 SWCNTs composed by 3-4 SWCNTs (Figure S12).

#### **CONCLUSION**

In conclusion, we have synthesized the SWCNT@BN van der Waals heterostructures from solution-processed chirality-pure SWCNTs, including (6,5), (7,5), and (8,4). We discovered an acid-facilitated SWCNT transfer method that enables the fabrication of free-standing, submonolayers of purified SWCNTs from the solutions as templates. The use of ADC, a thermally removable surfactant, made clean SWCNT surface accessible for the BN growth. The SWCNT@BN heterostructure exhibits PL of the inner SWCNTs but shows a spectral shift. Notably, the use of pure H<sub>2</sub> significantly improves the growth rate, while Cu is found to improve the crystallization of BN. This work provides a synthetic path to chirality pure SWCNT@BN heterostructures that are emerging experimental platforms for exploration of the chemistry and physics of one-dimensional van der Waals heterostructures.

#### **METHODS**

Certain commercial equipment, instruments or materials are identified in this paper in order to adequately specify experimental details. Such identification does not imply recommendation or endorsement by the National Institute of Standards and Technology (NIST), nor does it

imply that the materials or equipment are necessarily the best available for the purpose.

Fabrication of Free-Standing Purified SWCNT Films. (7,5)and (6,5)-SWCNTs were purified and sorted out by the ATPE method 12,29 from CoMoCAT SG65 family SWCNTs (Southwest Nanotechnologies/Chasm Nanotechnologies). Surfactants of the purified SWNCT solution were exchanged to 10.0 g/L ADC through ultrafiltration using a centrifugal filter unit (AmiconUltra-15, pore 100 kDa). In step 1, an AAO membrane (Whatman, diameter 25 mm, pore  $0.1 \mu m$ ) was placed on a fritted glass base assembled with a filter flask, which was connected to vacuum. ≈300 µL of water was added to wet the whole AAO membrane surface and then vacuum filtered. We then turned off the vacuum and added the SWCNT solution to the AAO membrane. The vacuum was then turned on to filter the solution and a thin SWCNT film was formed on the AAO membrane. We used 150  $\mu$ L solution of purified (6,5)-SWCNTs with an optical density (OD) of 1.52 at the E<sub>11</sub> wavelength (985 nm) to fabricate the 25 mm diameter (6,5)-SWCNT film, which had an optical transmittance of 93.1% at  $E_{11}$ . The (7,5)- and (8,4)-enriched SWCNT film, which had 86.3% transmittance at the E<sub>11</sub> wavelength (1033 nm) of (7,5), was prepared from 200  $\mu$ L solution with an OD of 1.81 at  $E_{11}$  of (7,5). Excess isopropanol (Sigma-Aldrich,  $\geq$  99.5%) and nanopure water were added on the AAO membrane and vacuum filtered to wash out the surfactant, followed by  $\approx$ 250  $\mu$ L of HCl (VWR, 36.5 to 38.0%). In step 2, the SWCNT thin film was released from the AAO by immersing the membrane in water. In step 3, we inserted a  $Si_3N_4$  (Norcada Inc., pore 20  $\mu$ m) grid into water below the floating film by using a tweezer to transfer the SWCNT film on the grid. To characterize the transmittance of the film, the SWCNT film was transferred to a glass slide for the absorption spectroscopy measurements (Figure S13), and the background from the glass slide was removed.

For EC2.0 SWCNTs (Meijo Nano Carbon Co. Ltd., >90%), which have a larger diameter ( $\approx$ 2 nm), the nanotube soot was used as received without further purification. The nanotubes were directly dispersed in 10.0 g/L ADC aqueous solution by tip sonication, and the resulting solution was then centrifuged to remove large undissolved bundles. The same procedure was used for the fabrication of EC2.0 SWCNT films.

**Synthesis of SWCNT@BN.** The  $Si_3N_4$  TEM grid with the suspended (6,5)-SWCNT film was placed on a quartz chip and tented with a Cu foil (purity 99.8%, thickness 0.025 mm, Alfa Aesar). The whole apparatus was placed at the center of a tube furnace (Figure S1). 10 mg of ammonia borane (97%, Sigma-Aldrich) was loaded upstream as the BN precursor, which was heated to 65 °C using a separate furnace. BN vapor was carried by a flow of 50 sccm of pure  $H_2$  to the zone where the grid was located, which had been heated to a temperature of 1065 °C for BN growth. The chamber pressure was maintained at 164 Pa. After 5 min, the process was stopped, and the power of the furnace was turned off. After the furnace cooled down to room temperature (approximately 2.5 h), the sample was taken out from the furnace.

For the control samples, we used the identical growth temperature (1065  $^{\circ}$ C), but the carrier gas (50 sccm of pure H<sub>2</sub> or 3 vol/vol % H<sub>2</sub>/Ar), Cu foil (used or not), and growth time (2, 5, or 30 min) were varied.

**Spectroscopic Characterization.** The optical absorption spectra of the SWCNT supernatants and the submonolayer SWCNT films were measured using an ultraviolet—visible—near-infrared spectrophotometer (PerkinElmer Lambda 1050) equipped with a broadband InGaAs detector. Raman spectra were measured on a Jobin-Yvon LabRam ARAMIS Raman microscope using 632.8 and 532 nm lasers operated at a power of 2 mW over a focused spot of  $\approx$ 0.8  $\mu$ m in diameter.

**TEM and EELS.** The suspended SWCNT@BN networks were characterized using a JEOL JEM 2100 LaB6 TEM with a 200 kV accelerating voltage. EELS mapping was performed by a JEM 2100 FE-TEM.

Hyperspectral Photoluminescence Imaging. The hyperspectral images and emission spectra were measured on a custom-

built microscope.<sup>30</sup> We used a continuous wave laser at 730 nm (Shanghai Dream Laser Technology Co., Ltd.) and 561 nm (JiveTM Cobolt AB, Sweden) as the excitation light sources. The images were captured using a  $50 \times$  or  $20 \times$  objective at an excitation power density of  $\approx 20-45$  W/cm², as specified in the caption for each figure.

#### **ASSOCIATED CONTENT**

#### **Supporting Information**

The Supporting Information is available free of charge at https://pubs.acs.org/doi/10.1021/acsnano.2c07128.

Schematic of the instrumental setup for the BN growth; statistics on the number of BN layers coating SWCNTs; additional TEM and EELS data; PL mappings; B-N bending mode observed in the Raman spectrum of SWCNT@BN; absorption spectra of (7,5)- and (8,4)-enriched SWCNT solution and submonolayer chirality-enriched SWCNT films (PDF)

#### **AUTHOR INFORMATION**

#### **Corresponding Author**

YuHuang Wang — Department of Chemistry and Biochemistry, University of Maryland, College Park, Maryland 20742, United States; Maryland NanoCenter, University of Maryland, College Park, Maryland 20742, United States; orcid.org/0000-0002-5664-1849; Email: yhw@umd.edu

#### **Authors**

Chiyu Zhang — Department of Chemistry and Biochemistry, University of Maryland, College Park, Maryland 20742, United States; orcid.org/0000-0001-6248-7879

Jacob Fortner – Department of Chemistry and Biochemistry, University of Maryland, College Park, Maryland 20742, United States

Peng Wang — Department of Chemistry and Biochemistry, University of Maryland, College Park, Maryland 20742, United States; orcid.org/0000-0003-0343-3920

Jeffrey A. Fagan — Materials Science and Engineering Division, National Institute of Standards and Technology, Gaithersburg, Maryland 20899, United States; orcid.org/ 0000-0003-1483-5554

Shuhui Wang — Department of Mechanical Engineering, The University of Tokyo, Tokyo 113-8656, Japan

Ming Liu — Department of Mechanical Engineering, The University of Tokyo, Tokyo 113-8656, Japan; ⊙ orcid.org/0000-0002-5630-3874

Shigeo Maruyama — Department of Mechanical Engineering, The University of Tokyo, Tokyo 113-8656, Japan; orcid.org/0000-0003-3694-3070

Complete contact information is available at: https://pubs.acs.org/10.1021/acsnano.2c07128

#### Notes

The authors declare no competing financial interest.

#### **ACKNOWLEDGMENTS**

This work was supported in part by the National Science Foundation (grant no. CHE2204202); the Center for Enhanced Nanofluidic Transport (CENT), an Energy Frontier Research Center funded by the U.S. Department of Energy, Office of Science, Basic Energy Sciences under award no. DE-SC0019112; JSPS KAKENHI (grant no. JP20H00220); and JST, CREST (grant no, JPMJCR20B5), Japan. J.A.F. was

funded by internal National Institute of Standards and Technology funds. We thank Dr. Sz-Chian Liou and Dr. Karen Gaskell for helpful discussions.

#### **REFERENCES**

- (1) Xiang, R.; Inoue, T.; Zheng, Y.; Kumamoto, A.; Qian, Y.; Sato, Y.; Liu, M.; Tang, D.; Gokhale, D.; Guo, J.; Hisama, K.; Yotsumoto, S.; Ogamoto, T.; Arai, H.; Kobayashi, Y.; Zhang, H.; Hou, B.; Anisimov, A.; Maruyama, M.; Miyata, Y.; Okada, S.; Chiashi, S.; Li, Y.; Kong, J.; Kauppinen, E. I.; Ikuhara, Y.; Suenaga, K.; Maruyama, S. One-Dimensional van der Waals Heterostructures. *Science* **2020**, *367*, 537–542
- (2) Feng, Y.; Li, H.; Inoue, T.; Chiashi, S.; Rotkin, S. V.; Xiang, R.; Maruyama, S. One-Dimensional van der Waals Heterojunction Diode. *ACS Nano* **2021**, *15* (3), 5600–5609.
- (3) Wang, P.; Zheng, Y.; Inoue, T.; Xiang, R.; Shawky, A.; Watanabe, M.; Anisimov, A.; Kauppinen, E. I.; Chiashi, S.; Maruyama, S. Enhanced In-Plane Thermal Conductance of Thin Films Composed of Coaxially Combined Single-Walled Carbon Nanotubes and Boron Nitride Nanotubes. *ACS Nano* **2020**, *14*, 4298–4305.
- (4) Gaviria Rojas, W. A.; Hersam, M. C. Chirality-Enriched Carbon Nanotubes for Next-Generation Computing. *Adv. Mater.* **2020**, *32*, 1905654.
- (5) Franklin, A. D. Nanomaterials in Transistors: From High-Performance to Thin-Film Applications. *Science* **2015**, 349 (6249), aab2750.
- (6) Geim, A. K.; Grigorieva, I. V. Van Der Waals Heterostructures. *Nature* **2013**, 499, 419–425.
- (7) Wang, J.; Ma, F.; Liang, W.; Sun, M. Electrical Properties and Applications of Graphene, Hexagonal Boron Nitride (h-BN), and Graphene/h-BN Heterostructures. *Materials Today Physics* **2017**, *2*, 6–34.
- (8) Shah, K. A.; Tali, B. A. Synthesis of Carbon Nanotubes by Catalytic Chemical Vapour Deposition: A Review on Carbon Sources, Catalysts and Substrates. *Materials Science in Semiconductor Processing* **2016**, *41*, 67–82.
- (9) Niyogi, S.; Hamon, M. A.; Hu, H.; Zhao, B.; Bhowmik, P.; Sen, R.; Itkis, M. E.; Haddon, R. C. Chemistry of Single-Walled Carbon Nanotubes. *Acc. Chem. Res.* **2002**, *35*, 1105–1113.
- (10) Nanot, S.; Hároz, E. H.; Kim, J.-H.; Hauge, R. H.; Kono, J. Optoelectronic Properties of Single-Wall Carbon Nanotubes. *Adv. Mater.* **2012**, *24*, 4977–4994.
- (11) Wang, P.; Barnes, B.; Huang, Z.; Wang, Z.; Zheng, M.; Wang, Y. Beyond Color: The New Carbon Ink. *Adv. Mater.* **2021**, *33*, 2005890
- (12) Subbaiyan, N. K.; Cambré, S.; Parra-Vasquez, A. N. G.; Hároz, E. H.; Doorn, S. K.; Duque, J. G. Role of Surfactants and Salt in Aqueous Two-Phase Separation of Carbon Nanotubes toward Simple Chirality Isolation. *ACS Nano* **2014**, *8*, 1619–1628.
- (13) Zheng, M.; Jagota, A.; Strano, M. S.; Santos, A. P.; Barone, P.; Chou, S. G.; Diner, B. A.; Dresselhaus, M. S.; Mclean, R. S.; Onoa, G. B.; Samsonidze, G. G.; Semke, E. D.; Usrey, M.; Walls, D. J. Structure-Based Carbon Nanotube Sorting by Sequence-Dependent DNA Assembly. *Science* **2003**, *302*, 1545–1548.
- (14) O'Connell, M. J.; Boul, P.; Ericson, L. M.; Huffman, C.; Wang, Y.; Haroz, E.; Kuper, C.; Tour, J.; Ausman, K. D.; Smalley, R. E. Reversible Water-Solubilization of Single-Walled Carbon Nanotubes by Polymer Wrapping. *Chem. Phys. Lett.* **2001**, 342, 265–271.
- (15) Xiang, R.; Maruyama, S. Heteronanotubes: Challenges and Opportunities. *Small Science* **2021**, *1*, 2000039.
- (16) Zheng, Y.; Kumamoto, A.; Hisama, K.; Otsuka, K.; Wickerson, G.; Sato, Y.; Liu, M.; Inoue, T.; Chiashi, S.; Tang, D.-M.; Zhang, Q.; Anisimov, A.; Kauppinen, E. I.; Li, Y.; Suenaga, K.; Ikuhara, Y.; Maruyama, S.; Xiang, R. One-Dimensional van Der Waals Heterostructures: Growth Mechanism and Handedness Correlation Revealed by Nondestructive TEM. *Proc. Natl. Acad. Sci. U.S.A.* **2021**, *118*, No. e2107295118.

- (17) Zhang, C.; Wang, P.; Barnes, B.; Fortner, J.; Wang, Y. Cleanly Removable Surfactant for Carbon Nanotubes. *Chem. Mater.* **2021**, *33*, 4551–4557.
- (18) Fagan, J. A. Aqueous Two-Polymer Phase Extraction of Single-Wall Carbon Nanotubes Using Surfactants. *Nanoscale Adv.* **2019**, *1*, 3307–3324.
- (19) Wu, Z.; Chen, Z.; Du, X.; Logan, J. M.; Sippel, J.; Nikolou, M.; Kamaras, K.; Reynolds, J. R.; Tanner, D. B.; Hebard, A. F.; Rinzler, A. G. Transparent, Conductive Carbon Nanotube Films. *Science* **2004**, 305, 1273–1276.
- (20) Yang, H.-C.; Xie, Y.; Chan, H.; Narayanan, B.; Chen, L.; Waldman, R. Z.; Sankaranarayanan, S. K. R. S.; Elam, J. W.; Darling, S. B. Crude-Oil-Repellent Membranes by Atomic Layer Deposition: Oxide Interface Engineering. *ACS Nano* **2018**, *12*, 8678–8685.
- (21) Liu, Z.; Zhang, J.; Gao, B. Raman Spectroscopy of Strained Single-Walled Carbon Nanotubes. *Chem. Commun.* **2009**, 45, 6902.
- (22) Aydin, M. Vibrational and Electronic Properties of Single-Walled and Double-Walled Boron Nitride Nanotubes. *Vib. Spectrosc.* **2013**, *66*, 30–42.
- (23) Arai, H.; Inoue, T.; Xiang, R.; Maruyama, S.; Chiashi, S. Non-Catalytic Heteroepitaxial Growth of Aligned, Large-Sized Hexagonal Boron Nitride Single-Crystals on Graphite. *Nanoscale* **2020**, *12*, 10399–10406.
- (24) Lu, J.; Ren, Q.; Sun, L.; Yu, J.; Chen, Y.; Shen, X.; Chen, Z. Temperature-Dependent Raman Spectra of Bamboo-like Boron Nitride Nanotubes. *Appl. Phys. Express* **2014**, *7*, 022401.
- (25) Wirtz, L.; Rubio, A. Optical and Vibrational Properties of Boron Nitride Nanotubes. In *B-C-N Nanotubes and Related Nanostructures*, Lecture Notes in Nanoscale Science and Technology; Springer: New York, 2009; pp 105–148.
- (26) Liu, M.; Hisama, K.; Zheng, Y.; Maruyama, M.; Seo, S.; Anisimov, A.; Inoue, T.; Kauppinen, E. I.; Okada, S.; Chiashi, S.; Xiang, R.; Maruyama, S. Photoluminescence from Single-Walled MoS2 Nanotubes Coaxially Grown on Boron Nitride Nanotubes. *ACS Nano* 2021, 15, 8418–8426.
- (27) Kumar, V.; Maity, P. C.; Lahiri, D.; Lahiri, I. Copper Catalyzed Growth of Hexagonal Boron Nitride Nanotubes on a Tungsten Substrate. *CrystEngComm* **2018**, *20*, 2713–2719.
- (28) Kim, K. K.; Hsu, A.; Jia, X.; Kim, S. M.; Shi, Y.; Hofmann, M.; Nezich, D.; Rodriguez-Nieva, J. F.; Dresselhaus, M.; Palacios, T.; Kong, J. Synthesis of Monolayer Hexagonal Boron Nitride on Cu Foil Using Chemical Vapor Deposition. *Nano Lett.* **2012**, *12*, 161–166.
- (29) Fagan, J. A.; Hároz, E. H.; Ihly, R.; Gui, H.; Blackburn, J. L.; Simpson, J. R.; Lam, S.; Hight Walker, A. R.; Doorn, S. K.; Zheng, M. Isolation of > 1 Nm Diameter Single-Wall Carbon Nanotube Species Using Aqueous Two-Phase Extraction. *ACS Nano* **2015**, *9*, 5377—5390.
- (30) Wu, X.; Kim, M.; Qu, H.; Wang, Y. Single-Defect Spectroscopy in the Shortwave Infrared. *Nat. Commun.* **2019**, *10*, 2672.

### **□** Recommended by ACS

## **Understanding Single-Walled Carbon Nanotube Growth for Chirality Controllable Synthesis**

Lu Qiu and Feng Ding

AUGUST 12, 2021

ACCOUNTS OF MATERIALS RESEARCH

READ 🗹

### Chirality Pure Carbon Nanotubes: Growth, Sorting, and Characterization

Feng Yang, Yan Li, et al.

FEBRUARY 10, 2020

CHEMICAL REVIEWS

READ 🗹

### Hexagonal Boron Nitride As an Ideal Substrate for Carbon Nanotube Photonics

N. Fang, Y. K. Kato, et al.

JUNE 02, 2020

ACS PHOTONICS

READ 🗹

### Origin of the Giant Enhanced Raman Scattering by Sulfur Chains Encapsulated inside Single-Wall Carbon Nanotubes

Viviane V. Nascimento, Cristiano Fantini, et al.

APRIL 26, 2021

ACS NANO

READ **C** 

Get More Suggestions >

#### **Supporting Information**

# Van der Waals SWCNT@BN Heterostructures Synthesized from Solution-Processed Chirality-Pure Single-Wall Carbon Nanotubes

Chiyu Zhang<sup>1</sup>, Jacob Fortner<sup>1</sup>, Peng Wang<sup>1</sup>, Jeffrey A. Fagan<sup>2</sup>, Shuhui Wang<sup>3</sup>, Ming Liu<sup>3</sup>, Shigeo Maruyama<sup>3</sup>, YuHuang Wang<sup>1,4</sup>\*

Certain commercial equipment, instruments or materials are identified in this paper in order to adequately specify experimental details. Such identification does not imply recommendation or endorsement by the National Institute of Standards and Technology (NIST), nor does it imply that the materials or equipment are necessarily the best available for the purpose.

This supporting information file includes 13 figures.

Figure S1: Schematic of the instrumental setup for the BN growth by chemical vapor deposition (CVD) method.

Figure S2: Statistics on the number of BN layers coating SWCNTs.

Figure S3, S5, S10, and S12: Transmission electron microscopy (TEM) data that demonstrate boron nitride (BN) protecting single-wall carbon nanotubes (SWCNTs) from electron beams, exhibit morphology of SWCNTs absorbed by surfactant from solutions and clean SWCNTs after annealing, compare the morphology of the heterostructure of single-wall carbon nanotube in boron nitride nanotube (SWCNT@BN) synthesized from various conditions, and show the morphology of SWCNT@BN with various inner SWCNT species.

Figure S6, S11: Electron energy-loss spectroscopy (EELS) that confirms growth of BN on the (7,5) and (8,4)-SWCNTs and proves that Cu does not accelerate the growth rate of BN.

Figure S7-8: Photoluminescence (PL) mappings show that the PL of (6,5)-SWCNTs disappear after high temperature treatment while the SWCNTs remain observable with scanning electron microscopy (SEM).

Figure S9: B-N bending mode observed in the Raman spectrum of (7,5)-SWCNT@BN.

<sup>&</sup>lt;sup>1</sup>Department of Chemistry and Biochemistry, University of Maryland, 8051 Regents Drive, College Park, MD 20742, USA

<sup>&</sup>lt;sup>2</sup>Materials Science and Engineering Division, National Institute of Standards and Technology, Gaithersburg, MD 20899, USA

<sup>&</sup>lt;sup>3</sup> Department of Mechanical Engineering, The University of Tokyo, Tokyo 113-8656, Japan

<sup>&</sup>lt;sup>4</sup>Maryland NanoCenter, University of Maryland, College Park, MD 20742, USA

<sup>\*</sup>email: yhw@umd.edu

Figure S4 and S13: Absorption spectra of (7,5)- and (8,4)-enriched SWCNT solution and submonolayer (6,5)-,(7,5)- and (8,4)-enriched SWCNT films, which are characterized by optical transmittance at the  $E_{11}$  peak of the SWCNTs."

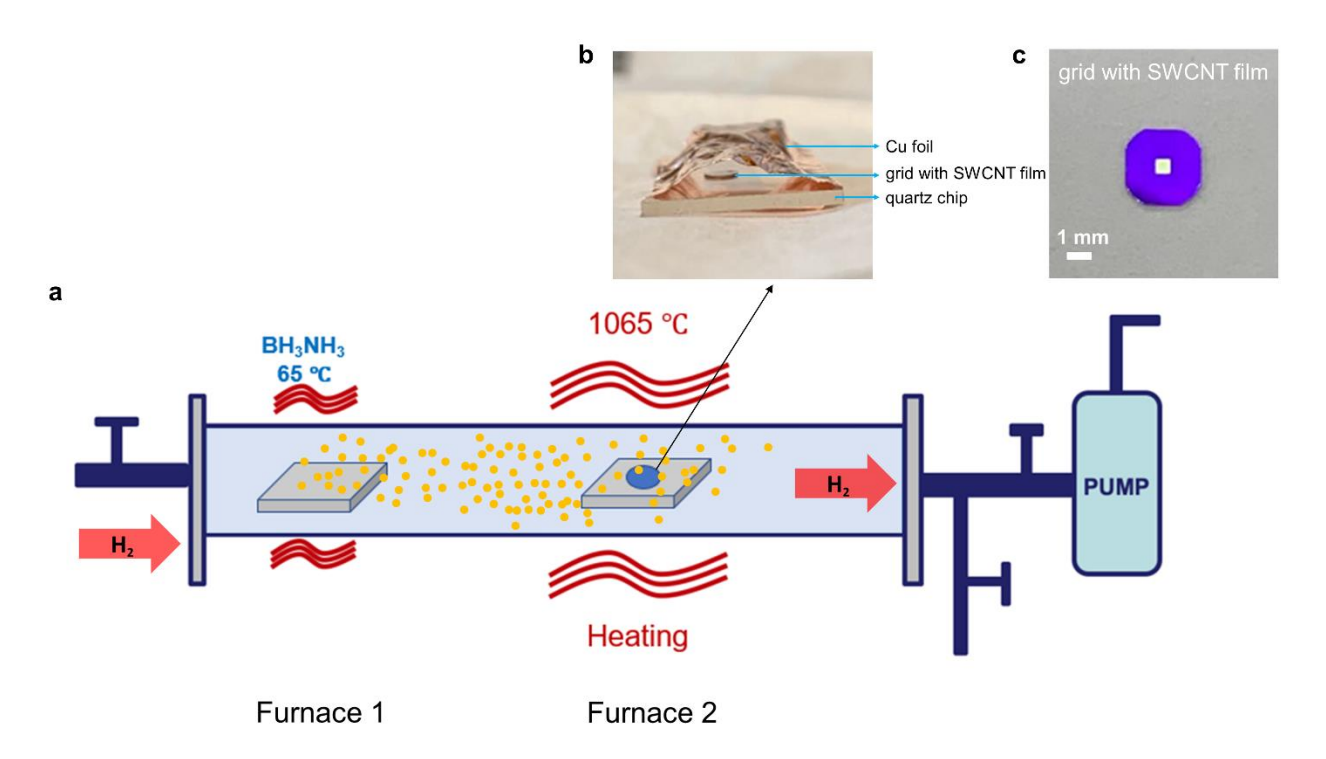


**Figure S1.** (a) Schematic of CVD set-up for synthesizing SWCNT@BN. Photo of (b) showing that a  $Si_3N_4$  grid is placed on a quartz chip and tented by a Cu foil and (c) the  $Si_3N_4$  grid with a suspended (6,5)-SWCNT film.

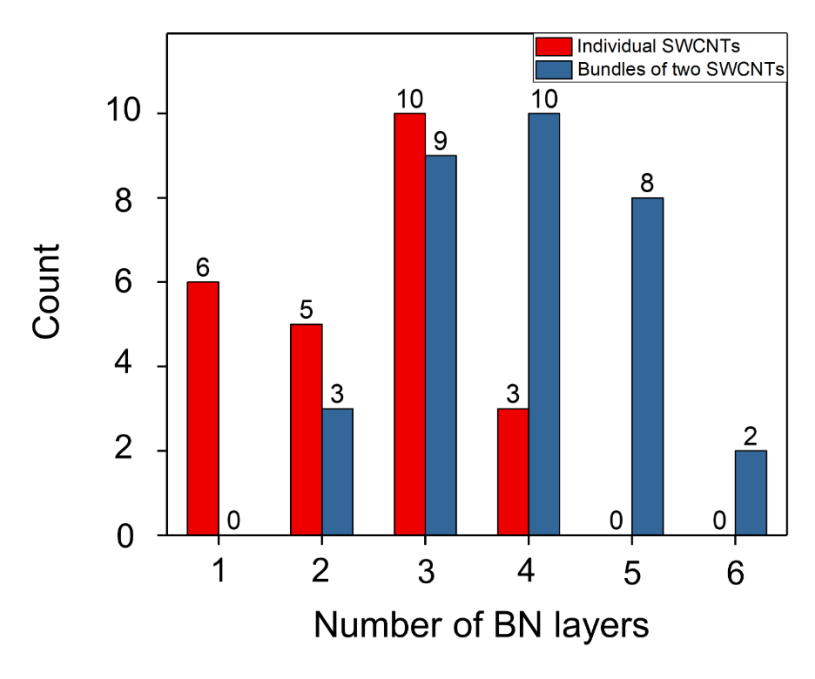


**Figure S2.** Number of BN layers coating SWCNTs. The histogram is constructed from a total of 56 isolated (6,5)-SWCNT@BN heterostructures, which contain either an individual SWCNT (red bars) or a two-nanotube bundle (blue bars). For heterostructures with varying BN layers along the length of a nanotube, the number of BN layers is measured from the thickest region.

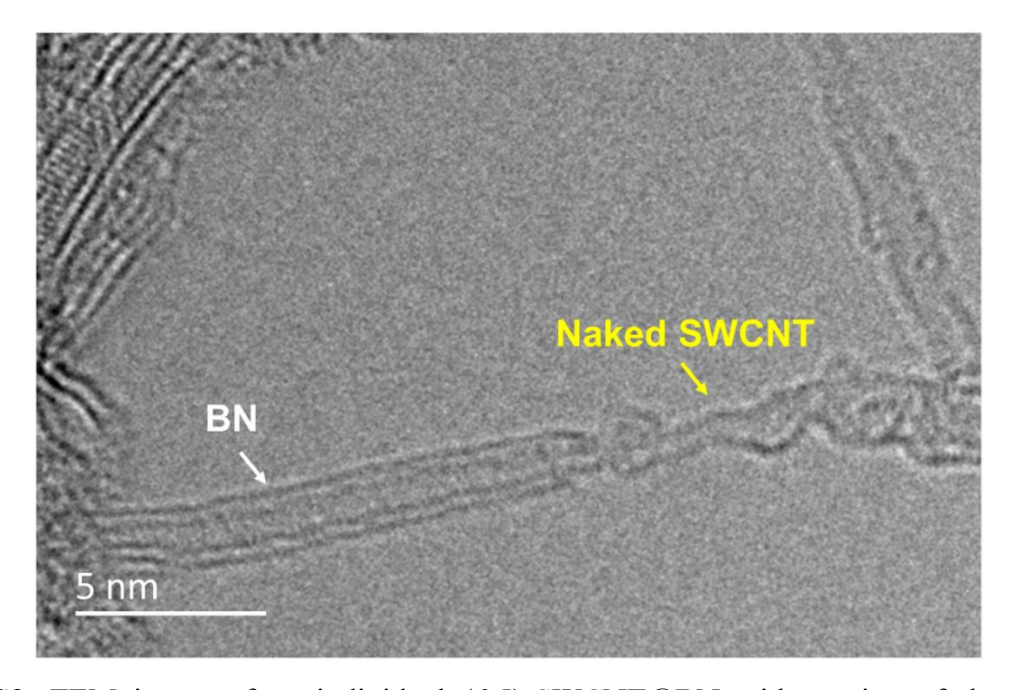


**Figure S3.** TEM image of an individual (6,5)-SWCNT@BN with portion of the nanotube protected by BN. The naked part of the (6,5) SWCNT is damaged by the TEM electron beam while the BN-protected part is intact.

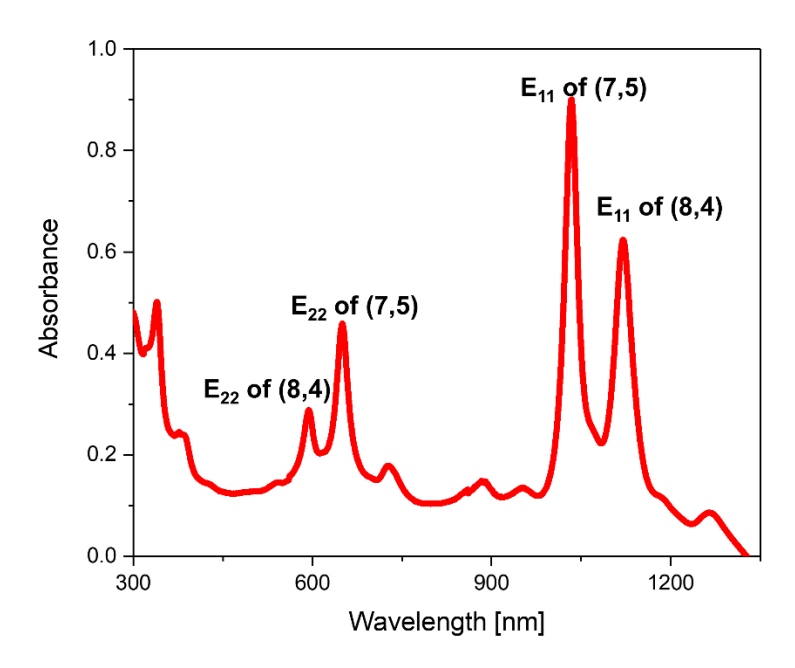


**Figure S4.** Absorption spectrum of (7,5) and (8,4)-enriched SWCNT solution. Due to the similar diameter, it is difficult to completely separated (8,4)-SWCNTs ( $E_{11} = 1121$  nm,  $E_{22} = 593$  nm) from (7,5)-SWCNTs ( $E_{11} = 1033$  nm,  $E_{22} = 649$  nm).

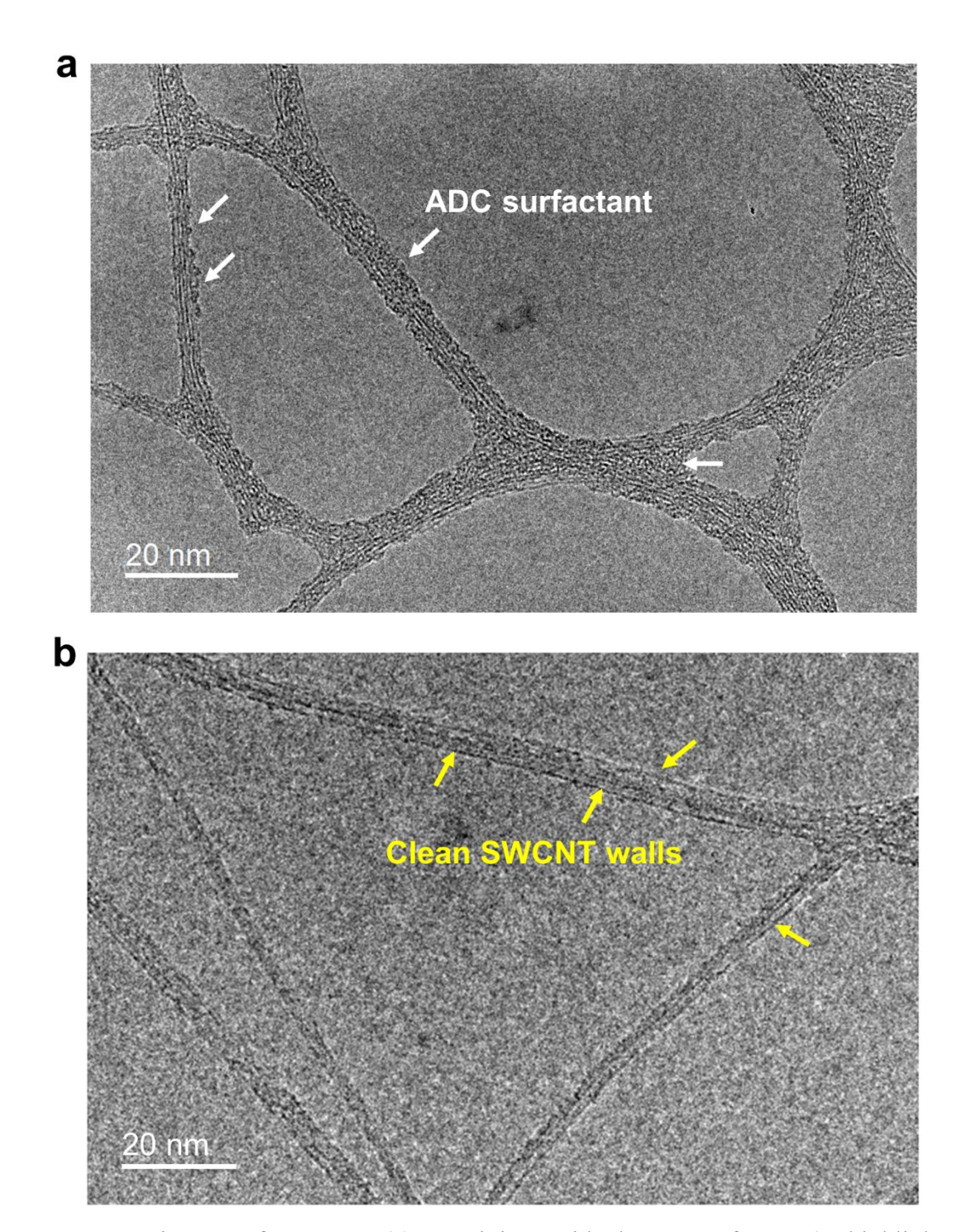


**Figure S5.** TEM images of SWCNTs (a) containing residual ADC surfactant (as highlighted by white arrows) before heat treatment and (b) exhibiting clean straight SWCNT walls (as highlighted by yellow arrows) after annealing in 3 vol/vol%  $H_2/Ar$  at 1065 °C for 30 min.

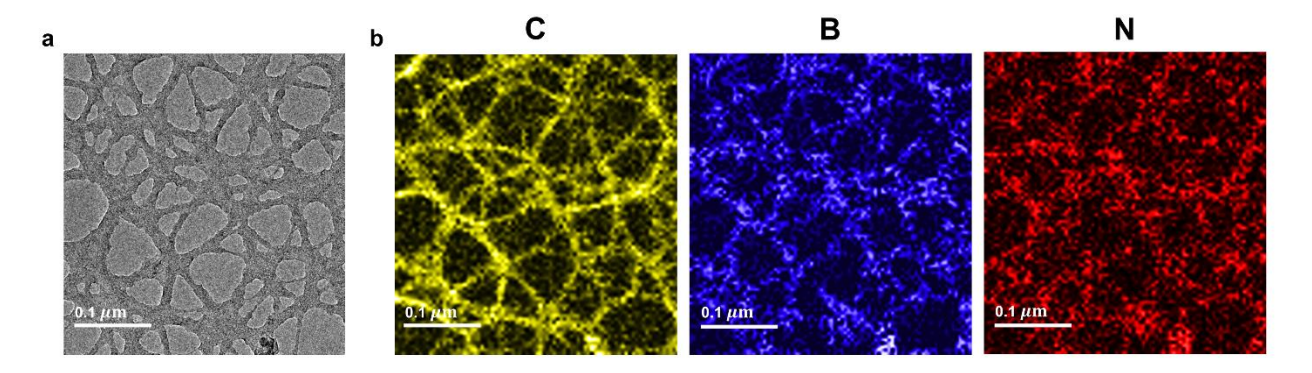


**Figure S6.** (a) TEM image of (7,5)- and (8,4)-SWCNT@BN networks and (b) corresponding EELS mapping of carbon, boron, and nitrogen.

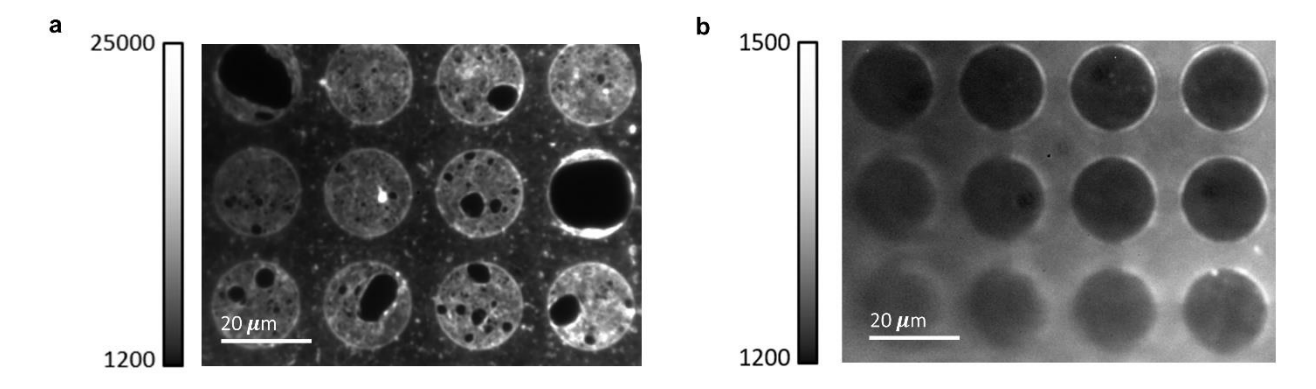


**Figure S7.** Hyperspectral PL images of the (6,5) SWCNT film (a) before and (b) after BN growth showing a nearly complete loss of the PL from the small diameter nanotube. The images were collected using a 561 nm laser at a power density of  $\approx 45 \text{ W/cm}^2$  and a 50x objective.

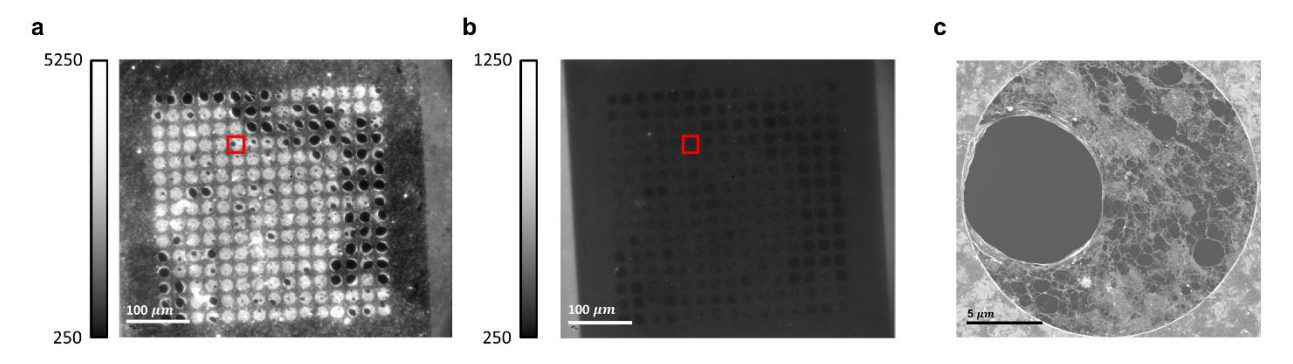


**Figure S8.** Hyperspectral images of (6,5) SWCNT film (a) before and (b) after annealing. The images were captured using a  $20^{\times}$  objective and a 561 nm laser at a power density of  $\approx 20 \text{ W/cm}^2$ . (c) SEM image of SWCNTs suspended over the pore in the red square in (a) and (b) after annealing.

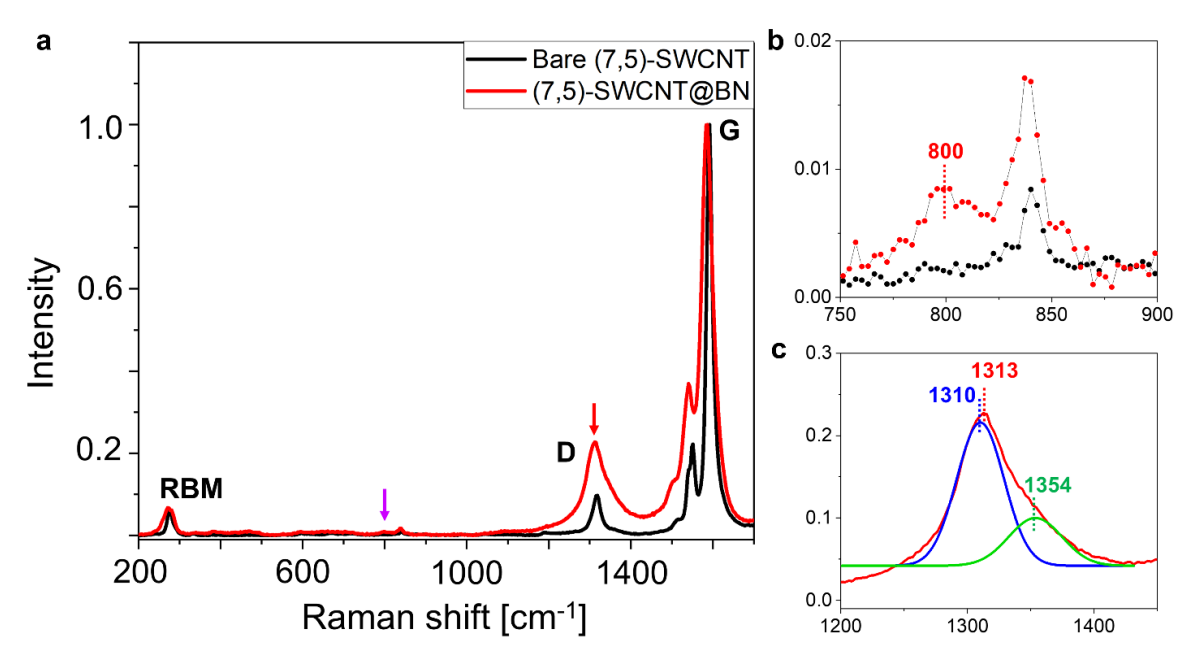


**Figure S9.** Raman spectra of (a) (7,5)-SWCNTs before (black) and after (red) BN growth. (b) A peak corresponding to B-N bending at 800 cm<sup>-1</sup> emerges after BN growth, which is marked by a purple arrow in (a). (c) The peak at 1313 cm<sup>-1</sup>, which is overlapped by the D peak of SWCNTs (blue curve, at 1310 cm<sup>-1</sup>) and B-N stretching peak (green, at 1354 cm<sup>-1</sup>), is marked by a red arrow in (a). The Raman excitation line is 632.8 nm.

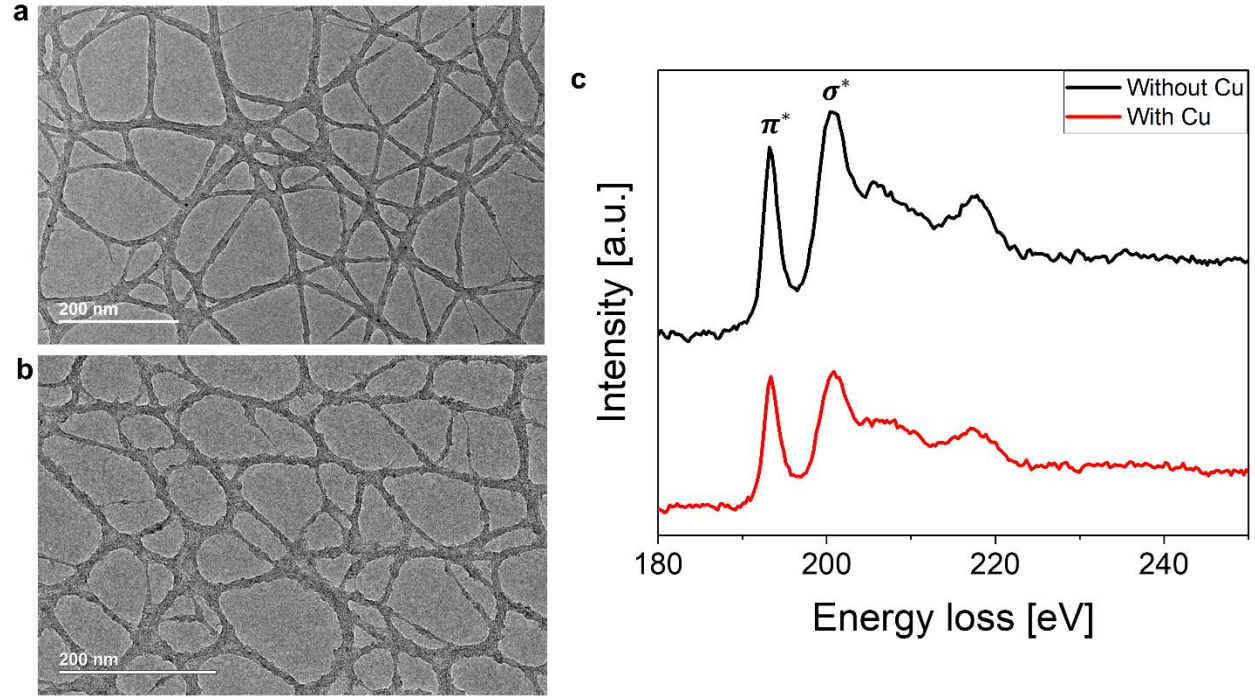


**Figure S10.** TEM images of the SWCNT@BN networks (a) grown with Cu in pure  $H_2$  for 2 min and (b) without Cu in 3 vol/vol %  $H_2$ /Ar for 30 min. (c) EELS spectra of boron atoms in the SWCNT@BN grown with Cu (red) and without Cu (black). The sample with Cu (red) shows a higher intensity ratio of  $\pi^*$  peak to the  $\sigma^*$  peak, indicating improved BN crystallization.

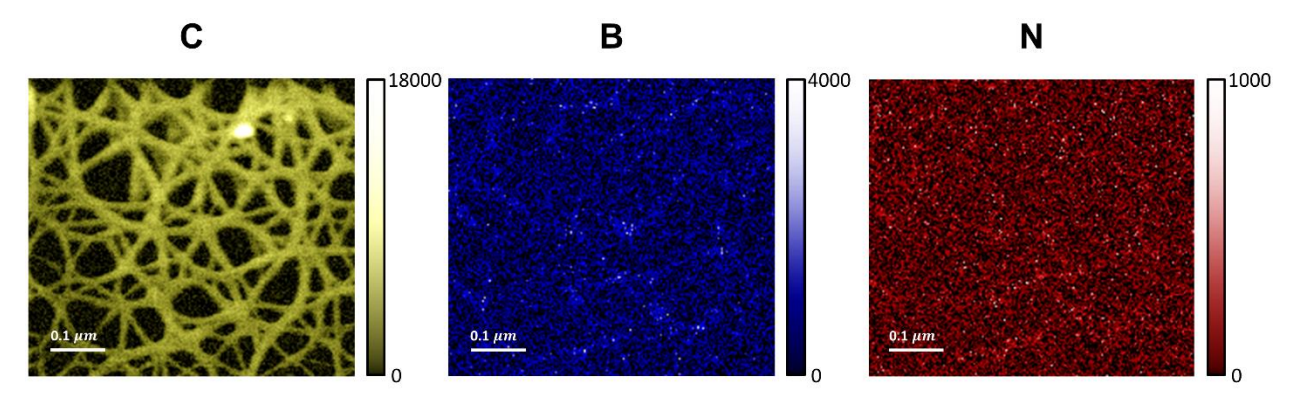


**Figure S11.** EELS mapping of carbon, boron, and nitrogen for a selected region of the (6,5)-SWCNT@BN sample synthesized in 3vol/vol % H<sub>2</sub> with Cu for 5 min. The weak signals of B and N indicate that BN did not develop in this condition.

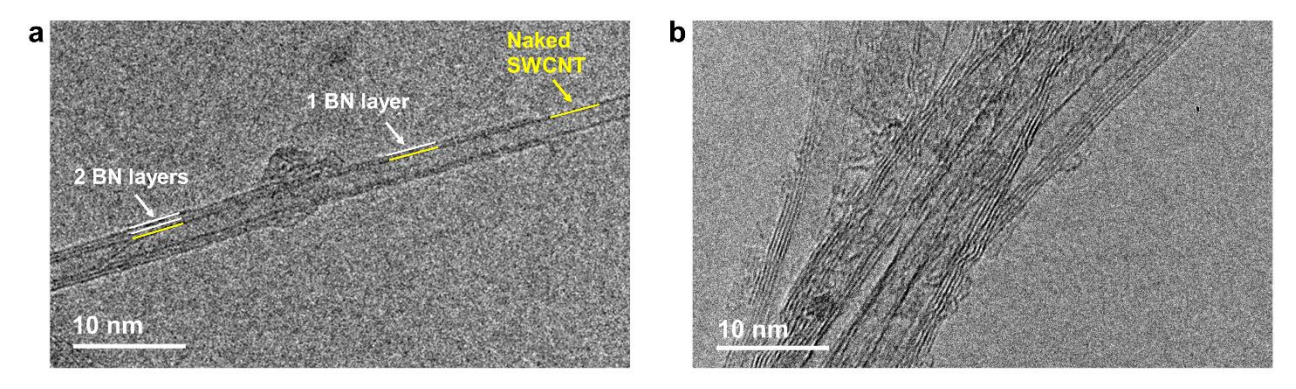


**Figure S12.** TEM images of (a) an individual EC2.0-SWCNT wrapped by 1-2 layers of BN and (b) a bundle of 3 to 4 EC2.0-SWCNTs wrapped by  $\approx$  4 layers after 2 min growth with Cu at 1070 °C.

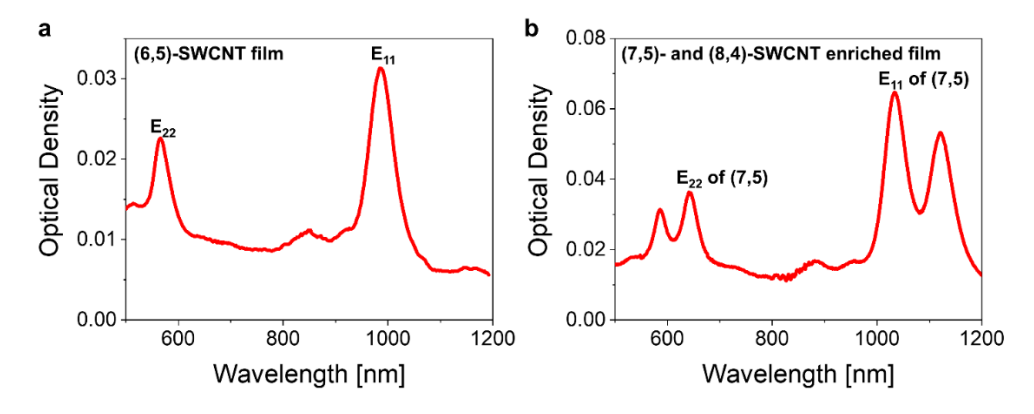


**Figure S13.** Absorption spectrum of sub-monolayer films made from (a) 150  $\mu$ L of purified (6,5)-SWCNT solution with an OD of 1.52 at the E<sub>11</sub> wavelength (985 nm) and (b) 200  $\mu$ L of (7,5)- and (8,4)- enriched SWCNT solution with an OD of 1.81 at the E<sub>11</sub> wavelength (1033 nm) of (7,5)-SWCNTs. The transmittance at E<sub>11</sub> wavelength of (6,5)-SWCNT is 93.1 % and of (7,5)-SWCNTs is 86.3%. Note that the film was released to water and transferred to a glass slide for the optical measurement.